Ensuring safety in hands-on control through stability analysis of the human-robot interaction

Luca Bascetta, Gianni Ferretti

Politecnico di Milano, Dipartimento di Elettronica, Informazione e Bioingegneria
Piazza Leonardo da Vinci 32, 20133 Milano, Italia

Abstract

This paper introduces a newly conceived methodology to design an admittance filter for hands-on control tasks, ensuring stability of human-robot interaction. Exploiting a nonlinear but simplified model of the human arm impedance, and a simple characterisation of the end-effector equivalent robot compliance, absolute stability theory allows to enforce a constraint on the design of the admittance filter damping. An experimental analysis, conducted on different subjects, allows to validate the human arm impedance model and determine the admittance filter parameters for linear and circular trajectories. Finally, hands-on control experiments reveal the absence of robot vibrations, induced by incipient instability, either in the robot measurements or in the feeling perceived by the human operator, and demonstrate that stability is guaranteed without causing an excessive human effort in the execution of the task.

Keywords: hands-on control, stability of human-robot interaction, human arm impedance model, admittance/impedance control

1. Introduction

In hands-on control, a typical example of physical human-robot interaction (pHRI), the human operator walks the robot through a desired path pushing and pulling the end-effector through a suitable handling device equipped with a force/torque sensor. In order to achieve this behaviour, the control system, that is usually constituted by one or more admittance filters, exploits the sensor

measurements to accommodate for the motion commanded by the operator.

From this description, it is evident that, during hands-on control tasks, human and robot are linked together and form a unique dynamical system, whose properties mainly depend on the mechanical properties of the human arm and of the robot mechanical chain. In particular, the stability of this system, a crucial property to guarantee a safe and comfortable human-robot interaction, cannot be inferred directly from the stability of the two separate systems, i.e., the human and the robot. In fact, assuming that the dynamics of the human arm are passive, a passive admittance filter is sufficient to ensure asymptotic stability of the closed-loop system [1] formed by the operator and the robot. Nevertheless, in many practical situations this assumption does not hold, and the robot, during the hands-on task, can exhibit severe vibrations, revealing the position control loop is close to the stability limit [2, 3, 4].

The popularity of hands-on control, as a technique to perform pHRI tasks, and its widespread dissemination in many different application fields, ranging from industrial robot programming [1, 5, 6, 7, 8] and cooperative lifting and moving of large payloads [9], to robotic surgery [10, 11], calls for a rigorous procedure to assess the stability of the human-robot interaction.

Considering human arm dynamics and arm mechanical impedance modelling, or pHRI and, in particular, admittance and impedance control, it must be noticed that an extremely rich literature exists. For example, many different control strategies have been developed to adapt or optimize the admittance/impedance filter parameters exploiting the robot redundancy [12], applying an online fast Fourier transform to the measured forces in order to detect and avoid incipient oscillations [13], using model-free continuous critic learning [14], proposing a variable impedance filter with online identification of the human arm stiffness [15], or using neural networks to learn online from data the robot and human arm models [4, 16, 17, 18]. On the other hand, different experimental devices and protocols have been also created to investigate the characteristics of the human operator during admittance and impedance controlled tasks [19, 20, 21].

Nevertheless, none of the previous works has addressed the problem of human-robot stability, i.e., hands-on control oscillations, in a unified way, considering a realistic model of the human arm mechanical impedance, that can be identified from experimental data using the same robot and sensor adopted to perform the hands-on control task, and proposing a theoretically grounded methodology to tune the admittance filter parameters ensuring the stability of the human-robot interaction.

To partially weaken the statement above, it must be noticed that a paper considering human-robot interaction stability under admittance control has been published very recently [22]. This work, however, considers only a single degree of freedom rigid mechanical system, subject to velocity and admittance control, and assumes that the human arm is characterised by passive dynamics, i.e., interaction stability can be guaranteed if the controlled mechanical system is passive as well. As a consequence of the aforementioned assumptions, the authors conclude that the stability conditions are too conservative, and imply a strong limitation on the velocity loop integral action, thus limiting the control performance of the mechanical system. Even the alternative methodology proposed to overcome these limitations, however, being based on linear system's analysis tools, cannot be applied to multi-link manipulators or realistic nonlinear human arm impedance models.

The aim and contribution of this work is to fill the mentioned gap, devising a stability analysis of the human-robot system, based on a nonlinear model of the human arm and on the absolute stability theory, that allows to tune the admittance filter parameters ensuring stability of the human-robot interaction during hands-on control tasks. The work includes also an experimental campaign that shows the identification of the human arm impedance parameters, the admittance filter tuning, and a validation of the proposed methodology through hands-on control tests along linear and curvilinear paths. Moreover, a way to exploit the human arm nonlinear model to draw damping charts that reveal the most critical areas in the robot workspace, in terms of stability of the human-robot interaction, is presented, as well. Finally, the proposed tun-

ing methodology opens the way to the design of an adaptive admittance filter that, thanks to a continued online human arm impedance identification, ensures robust asymptotic stability and accuracy of the hands-on control task.

The paper is organized as follows. Section 2 formulates the problem of assessing the stability of human-robot interaction during hands-on control tasks. Section 3 introduces the two human arm models used in the paper. The first one, more complex, that is exploited to simulate the human arm impedance, and the second one, simplified, that is exploited in Section 4 to study the absolute stability of the human-robot system and to derive a design methodology to tune the admittance filter parameters. Section 5 describes the experimental activity performed to identify the human arm impedance parameters, and reports the results of some hands-on control experiments demonstrating the effectiveness of the proposed methodology in providing a tuning of the admittance filter that ensures absence of undesired vibrations during hands-on control tasks. Conclusions are drawn in Section 6.

2. Problem formulation

In hands-on control or walk-through programming, the human operator plays the role of a teacher that physically walks the robot through the desired path. The physical interaction between the operator and the robot has to be conceived in such a way that he/she has the impression to grab a real tool instead of the robot end-effector. The role of the control system is thus to accommodate for the motion commanded by the operator, mimicking the same dynamic behaviour of the real tool, i.e., behaving like a virtual tool that exhibits the same mechanical properties of the real tool [1].

For these reasons, hands-on control techniques are usually based on admittance control [1], a control strategy that is implemented closing an external loop outside the position control loops of the industrial robot controller (Figure 1). The admittance controller is fed by forces and moments exerted by a human operator, measured by a force/torque sensor mounted at the end-effector, and determines

modifications to the Cartesian references in order to guarantee the prescribed compliant behaviour. As a consequence, during hands-on control the human

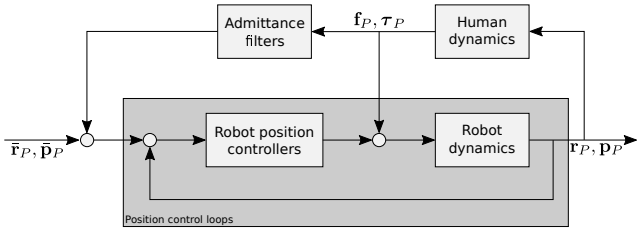

Figure 1: Control architecture for admittance control. $\mathbf{f}_P$ and $\boldsymbol{\tau}_P$ are the forces and torques exerted by human hand, respectively; $\mathbf{p}_P$ ($\bar{\mathbf{p}}_P$) and $\mathbf{r}_P$ ($\bar{\mathbf{r}}_P$) are the end-effector (reference) Cartesian position and (reference) orientation, respectively.

operator is closing a further loop outside the industrial controller position loops (Figure 1) that, in particular situations, depending on the impedance properties of the robot mechanical chain and the human arm, and on the admittance filter tuning, can lead to severe robot vibrations or even instability.

In order to simplify the stability analysis of the hands-on control task, it is usually assumed that the dynamics of the human arm are passive and, thus, a passive admittance filter is sufficient to ensure asymptotic stability of the closed loop system [1]. In many practical situations, however, this simplification occurs to be too rough as the robot during the hands-on task can exhibit severe vibrations, revealing the position control is close to the stability limit.

For these reasons, a thorough stability analysis and a methodology to tune the admittance filters in order to ensure stability, as much as possible independently of the specific human operator characteristics, are in order.

To this extent, a simplification of the control architecture in Figure 1 is required. A closer analysis reveals that there is a neat frequency separation between human dynamics and position control loops, whose response is from ten to twenty times faster with respect to the human dominant dynamics [23]. For this reason, one can assume that the effects of human torques and forces, acting on the robot control loops as disturbances, are completely rejected by the industrial robot controller. Furthermore, the relation between the reference and

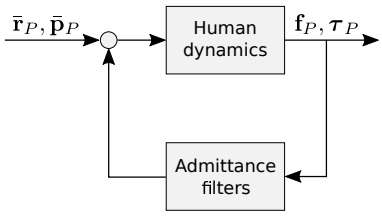

Figure 2: Simplified control architecture for stability analysis.$\mathbf{f}_P$ and $\boldsymbol{\tau}_P$ are the forces and torques exerted by human hand, respectively; $\bar{\mathbf{p}}_P$ and $\bar{\mathbf{r}}_P$ are the end-effector reference Cartesian position and orientation, respectively.

actual robot pose, thanks to the aforementioned frequency separation and to the properties of a cascaded control architecture, i.e., the standard control structure applied in motion control systems, can be approximated with a unitary transfer function.

As a consequence, the admittance control architecture can be simplified, for the sake of the stability analysis, to a closed-loop system having the human dynamics in the feed-forward path and the admittance filters in the feedback path (Figure 2). Starting from this formulation, once a suitable model of the human dynamics has been defined (see Section 3 for further details), a stability analysis based on the so called "Lur'e problem" [24] can be introduced (see Section 4 for further details).

3. Human arm model

This section focuses on the derivation of a model of the human arm dynamics suitable for stability analysis and for a preliminary validation of the methodology here proposed.

First of all, it must be noticed that the contribution of the human operator to the system dynamics and to the impedance of the mechanical chain is mainly related to the human arm [15, 25]. For this reason only the human arm mechanical impedance is here considered.

Furthermore, differently from a robot, modelling a human arm is a very complex task, depending on a huge number of parameters that can be time varying or

may depend on the single person, and are often unmeasurable or very difficult to be measured [26]. The complexity is further increased by the fact that an accurate model of the human arm should consider not only mechanical characteristics but also neuromuscular properties [27, 28, 29].

The aim of this section is thus to introduce two simplified human arm models, including mechanical and neuromuscular properties, able to represent the equivalent mechanical impedance at the operator hand, i.e., the impedance seen by the robot. The first one, targeted to simulation, is more accurate and considers a complete visco-elastic characterization. The second one, instead, aiming at stability analysis, is more simple and includes only the elastic effect.

The two models are derived under the following assumptions:

- the operator hand performs a translational[1] planar motion;
- the human arm mechanical impedance in the motion plane can be decomposed into two contributions, along the x and y directions, respectively;
- an isotropic human arm impedance model is adopted.

The introduction of these assumptions, that are common to all the relevant literature on human-robot interaction, does not affect the validity of the model, as it is demonstrated by the experimental results reported in Section 5, but greatly simplifies its derivation and especially the parameter identification phase.

According to the previous assumptions, the complete force-displacement relation, that models the mechanical behaviour of the human arm along the x and y directions, is represented by the following second order differential equation [15, 30, 31]

$$\mathbf{F}_h\left(\mathbf{q}_h, t\right) = \mathbf{M}_h(\mathbf{q}_h, t)\ddot{\mathbf{q}}_h + \mathbf{D}_h(\mathbf{q}_h, t)\dot{\mathbf{q}}_h + \mathbf{K}_h(\mathbf{q}_h, t)\mathbf{q}_h \tag{1}$$

where $\mathbf{F}_h\left(\mathbf{q}_h, t\right)$ is the force exerted by the human arm at the hand frame in the x and y directions, $\mathbf{M}_h(\mathbf{q}_h, t)$, $\mathbf{D}_h(\mathbf{q}_h, t)$ and $\mathbf{K}_h(\mathbf{q}_h, t)$ are the time-varying

[1] Though the model could be easily extended to consider rotational impedance, for the sake of simplicity this work is focused only on the translational one.

and configuration dependent equivalent mass, damping and stiffness matrices related to the x and y directions, respectively, and $\mathbf{q}_h = [x \;\; y]^T$.

Considering stiffness, experimental results [15, 26, 32] reveal that its effect is dominant with respect to the viscous and inertial one, and that the spatial components of the stiffness matrix are coupled, i.e., $\mathbf{K}_h(\mathbf{q}_h, t)$ is a non-diagonal matrix. Consequently, the stiffness matrix can be decomposed into a symmetric and an anti-symmetric component, but under the assumption of planar motion the symmetric component represents the dominant effect [26, 32]. Finally, the symmetric component has directional properties and can be represented as an ellipsoid, whose axis lengths and directions depend on the eigenvalues and eigenvectors respectively, rotated in such a way that the principal axis is directed along the line that passes through the wrist and the shoulder [26]. A similar directional property characterises mass and damping, as well.

As for damping, it has been shown [23, 33, 34] that it is strictly related to human arm stiffness and can be modelled using the following relation

$$\mathbf{D}_h(\mathbf{q}_h, t) = \begin{bmatrix} \delta_{xx}\sqrt{K_{h_{xx}}(\mathbf{q}_h, t)} & 0 \\ 0 & \delta_{yy}\sqrt{K_{h_{yy}}(\mathbf{q}_h, t)} \end{bmatrix}$$

where $\delta_{xx}, \delta_{yy} \in [0, 1]$ are weighting factors, and $K_{h_{xx}}(\mathbf{q}_h, t)$, $K_{h_{yy}}(\mathbf{q}_h, t)$, are the diagonal elements of the stiffness matrix.

As previously mentioned, the human arm behaviour depends either on its mechanical characteristics and on neuromuscular properties. The model introduced in (1) has thus to be integrated considering the most relevant neuromuscular properties, i.e., reaction times associated to voluntary and involuntary movements, and effect of muscle co-contraction.

First of all, human reactions, either voluntary or involuntary, are characterised by a reaction time ranging from 150 to 200 ms for voluntary movements [27], and from 50 to $100 - 200$ ms for involuntary movements [8, 27, 35].

On the other side, co-contraction is a voluntary or involuntary simultaneous isometric contraction of the agonist and antagonist muscles that generates an increase of the hand Cartesian stiffness [36, 26]. The reaction time associ-

ated to involuntary co-contraction, the only one considered in this work, ranges from 30 ms, for primary reflexes, to $100 - 200$ ms, for secondary or postural reflexes [8, 27, 35].

In order to take into account the effects of these neuromuscular properties, stiffness can be decomposed into two components as follows [25]

$$\mathbf{K}_h(\mathbf{q}_h, t) = \mathbf{K}_{post}(\mathbf{q}_h, t) + \mathbf{K}_{cont}(t)$$

where the first contribution is related to postural stiffness, and depends only on the arm configuration, and the second one to the co-contraction phenomenon, and depends only on the level of co-contraction. In the case of planar hand motion and involuntary co-contraction, it can be shown [25] that stiffness due to co-contraction can be modelled as

$$\mathbf{K}_{cont}(t) = \bar{\mathbf{K}}_{cont}\sigma(t - \tau)$$

where $\bar{\mathbf{K}}_{cont}$ is the maximum stiffness increase due to co-contraction, $\sigma : \mathbb{R} \to [0, 1]$ is a normalized muscular co-contraction index, and τ is a delay accounting for involuntary reaction time.

On the other hand, experiments [37] show that postural stiffness, in case of planar hand motion, can be decomposed into two components related to two orthogonal axes, each one modelled as a quadratic function of the position along the corresponding axis, i.e., for the x axis

$$K_{post_x}(x, t) = b_1 x^2(t) + b_2 x(t) + b_3$$

where b_1, b_2, and b_3 represent suitable coefficients.

From a stability analysis point of view, model (1) can be simplified neglecting damping and inertia effects [25]. In fact, on one side damping has always a stabilising effect, as a consequence considering only the stiffness component is equivalent to analyse a worst case scenario; on the other side, as in hands-on control tasks the human arm accelerations are rather low, stiffness effect is dominant with respect to inertia.

A further simplification can be introduced, again in the direction of considering

the worst case scenario, associating the same involuntary reaction time τ to the postural stiffness, as well.

In conclusion, the impedance model adopted for stability analysis along the x direction is given by

$$F_h(x,t) = b_1 x^2(t-\tau) + b_2 x(t-\tau) + b_3 + a\sigma(t-\tau) \tag{2}$$

where a is the maximum stiffness increase in the x direction due to co-contraction, i.e., $a = \bar{K}_{cont_x}$.

4. Stability analisys of human-robot interaction

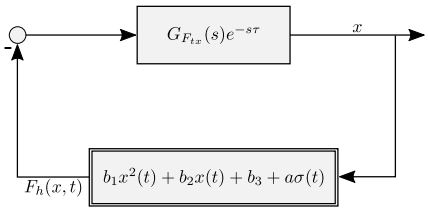

Figure 3: The closed-loop system for absolute stability analysis.

Considering the simplified control architecture reported in Figure 2, one can observe that:

- during hands-on control tasks, external reference inputs $\bar{\mathbf{p}}_P$ and $\bar{\mathbf{r}}_P$, i.e., position and orientation reference values, respectively, are always zero;
- translational admittance filters can be represented by a diagonal transfer matrix, where each transfer function is a second order mass-damping system[2];
- human arm dynamics, for the sake of stability analysis, can be represented by a diagonal matrix where each diagonal element, modelling the

[2]The same holds for rotational admittance [1] but, according to the assumptions introduced in Section 3, only translational motion is here considered.

human arm translational impedance in one Cartesian direction, is given by relation (2).

Under the previous assumptions, the block diagram in Figure 2 is composed by two independent closed-loop systems. As a consequence, the stability analysis can be performed considering each motion direction separately.

The problem of assessing the stability of the human-robot interaction during an hands-on control task can be formalised as the problem of analysing the stability of the SISO closed-loop system in Figure 3, where:

- $G_{F_{tx}}(s)$ is the transfer function of the admittance filter for a translational motion along the x direction, defined as follows

$$G_{F_{tx}}(s) = \frac{1}{M_x s^2 + D_x s}$$

  where M_x and D_x are the virtual tool translational mass and damping in the x direction, respectively;

- τ accounts for the delay introduced by the involuntary reaction time;

- the feedback block represents the simplified human arm nonlinear impedance model excluding the delay that has been added to the linear part of the closed-loop system.

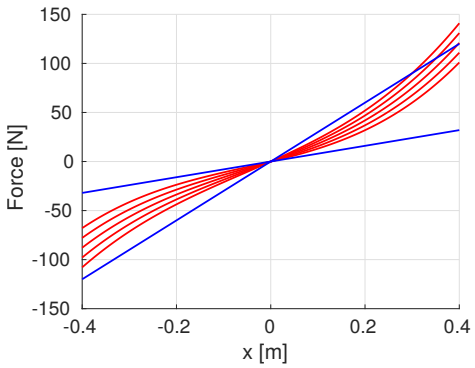

Figure 4: An example of sector nonlinearity $F_h(x,t)$ obtained with $b_1 = 600$, $b_2 = 103.\bar{3}$, $b_3 = 115$, $a = 100$, and for co-contraction index equal to 0, 0.25, 0.5, 0.75, and 1.

In order to recast the stability analysis into a Lur'e problem, for any given $\sigma(t)$, the nonlinear feedback

$$\begin{aligned} F_h(x,t) &= K_h(x,t)x(t) \\ &= \left(b_1 x^2(t) + b_2 x(t) + b_3 + a\sigma(t)\right) x(t) \end{aligned}$$

being a memoryless time-varying nonlinearity, piecewise continuous in t and locally Lipschitz in x, has to satisfy the following sector condition [24]

$$\alpha x^2 \leq x F_h(x,t) \leq \beta x^2 \qquad \forall t > 0 \tag{3}$$

where α, $\beta \in \mathbb{R}$, $\alpha < \beta$, and $x \in [x_{min}, x_{max}]$, with $x_{min} < 0 < x_{max}$, x_{min} and x_{max} determining the range of x values for which one is interested to prove the absolute stability of the closed-loop system. Figure 4 shows an example where for $x \in [-0.3, 0.3]$ the human arm stiffness has been bounded between $80\,x$ and $300\,x$. It is straightforward to verify that, for any reasonable parametrisation of $K_h(x,t)$, two constants α and β can be always determined such that (3) is verified (see Section 5 for further details).

Moreover, note that stability robustness is strictly related to the distance between $F_h(x,t)$ and the boundaries αx and βx.

On the other hand, the linear system in Figure 3, i.e., the impedance filter $G_{F_{tx}}(s)$, must be an asymptotically stable and finite dimensional system. In order to cope with these constraints, the delay can be substituted with its Padé approximation, i.e., considering a first order Padé approximation[3]

$$G(s) = G_{F_{tx}}(s)e^{-s\tau} \approx \frac{1}{M_x s^2 + D_x s} \frac{1 - s\tau/2}{1 + s\tau/2}$$

and pole shifting can be applied in order to make $G(s)$ asymptotically stable, introducing

$$G_T(s) = \frac{G(s)}{1 + \alpha G(s)}$$

[3]It can be easily shown [38], that a first order approximation is sufficient, i.e., increasing the order the result of the stability analysis, even in terms of the minimum damping ensuring stability, does not change.

where α is one of the coefficients defining the boundaries of the sector nonlinearity.

Using absolute stability theory [24], one can demonstrate that the closed-loop system in Figure 3 is absolutely stable within a finite domain $x \in [x_{min}, x_{max}]$ if

$$Z_T(s) = 1 + (\beta - \alpha)G_T(s) = \frac{1 + \beta G(s)}{1 + \alpha G(s)}$$

is strictly positive real, α and β being again the coefficients defining the boundaries of the sector nonlinearity.

In turn, $Z_T(s)$ is strictly positive real if and only if $Z_T(s)$ is asymptotically stable and

$$\mathrm{Re}\left[\frac{1 + \beta G(j\omega)}{1 + \alpha G(j\omega)}\right] > 0 \qquad \forall \omega \in \mathbb{R}$$

The last condition holds if the Nyquist plot of $G(j\omega)$ does not enter the disk in the complex plane whose center is on the real axis and crosses the real axis at $-1/\alpha$ and $-1/\beta$.

The previous analysis can be used to verify if a given parametrisation of the admittance filter guarantees the stability of the human-robot interaction. On the other side, the same procedure can be adopted, once the mass M_x has been selected, to determine the minimum damping D_x ensuring stability of the human-robot interaction.

Figure 5 shows an example of application of this methodology. Assuming a sector nonlinearity bounded by $\alpha = 80$ and $\beta = 300$, and a human impedance characterised by a mass $M_x = 2\,\mathrm{Kg}$ and a reaction time $\tau = 100\,\mathrm{ms}$, transfer functions $G(s)$, $G_T(s)$ and $Z_T(s)$ are given by

$$\begin{aligned} G(s) &= \frac{1 - 0.05s}{(2s^2 + D_x s)\,(1 + 0.05s)} \\ G_T(s) &= \frac{1 - 0.05s}{0.1s^3 + (2 + 0.05D_x)\,s^2 + (D_x - 4)\,s + 80} \\ Z_T(s) &= \frac{0.1s^3 + (2 + 0.05D_x)\,s^2 + (D_x - 15)\,s + 300}{0.1s^3 + (2 + 0.05D_x)\,s^2 + (D_x - 4)\,s + 80} \end{aligned}$$

An iterative procedure can be now applied, starting from a low damping and increasing it until the Nyquist plot of $G(j\omega)$ does not enter any more the disk

in the complex plane whose center is on the real axis and crosses the real axis at $-1/\alpha$ and $-1/\beta$. Figure 5 shows a sequence of 4 iterations, starting from a damping of 10 Ns/m (Figure 5(a)) and increasing its value until the Nyquist plot is tangent to the disk (Figure 5(d)), corresponding to a damping of 32 Ns/m. This last value represents the minimum damping D_x ensuring stability of the human-robot interaction.

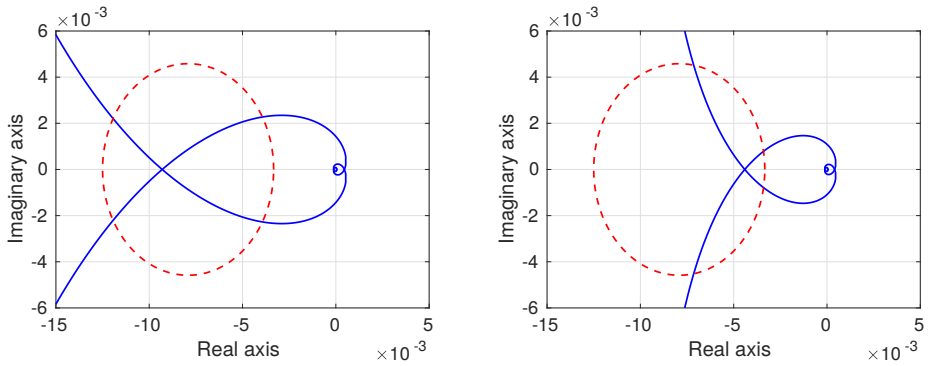

(a) $D_x = 10\,\mathrm{Ns/m}$ (b) $D_x = 20\,\mathrm{Ns/m}$

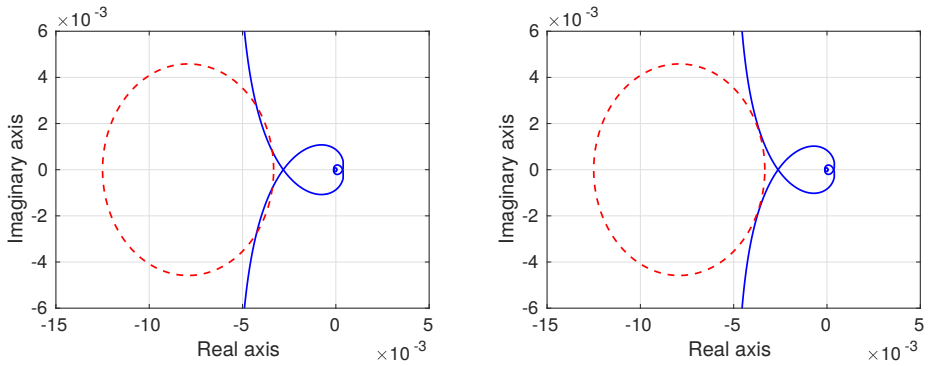

(c) $D_x = 30\,\mathrm{Ns/m}$ (d) $D_x = 32\,\mathrm{Ns/m}$

Figure 5: An example of stability analysis.

Nevertheless, it must be considered that the procedure herein described neglects an important aspect, sometime crucial in determining the stability of the human-robot interaction, that is the robot flexibility at joint and link levels. To

cope with this issue the linear system in Figure 3 has to be modified, introducing the equivalent end-effector Cartesian mass and stiffness of the robot.
Considering again a translation in the x direction, the dynamics of the impedance filter, together with the mass-spring system representing the equivalent mechanical characteristics of the robot at the end-effector, are represented by the following second order system

$$\begin{aligned} M_x\ddot{x}_1 + D_x\dot{x}_1 + K_{r_x}(x_1 - x_2) &= 0 \\ M_{r_x}\ddot{x}_2 + K_{r_x}(x_2 - x_1) &= -K_h(x_2,t)x_2 = -F_h(x_2,t) \end{aligned}$$

where M_{r_x} and K_{r_x} are the equivalent end-effector Cartesian mass and stiffness of the robot, respectively, and x_1, x_2 are the end-effector and hand positions, respectively.
Applying the Laplace transform and solving with respect to the human hand position x_2 one obtains the following modified expression of $G_{F_{tx}}(s)$

$$G_{F_{tx}}(s) = \frac{M_x s^2 + D_x s + K_{r_x}}{(M_x s^2 + D_x s + K_{r_x})(M_{r_x} s^2 + K_{r_x}) - K_{r_x}^2}$$

that has to be substituted to the previous admittance filter transfer function.
In order to perform the stability analysis in this case as well, suitable relations to derive the equivalent end-effector Cartesian mass and stiffness of the robot have to be introduced.
The equivalent mass M_{r_j} in the j-th Cartesian direction ($j = x, y, z$), depending on the robot configuration $\mathbf{q}$, is given by [39]

$$M_{r_j} = \frac{1}{\mathbf{e}_j^T \left[\mathbf{J}(\mathbf{q})\mathbf{B}^{-1}(\mathbf{q})\mathbf{J}^T(\mathbf{q})\right]\mathbf{e}_j}$$

where $\mathbf{J}(\mathbf{q})$ and $\mathbf{B}(\mathbf{q})$ are the geometric Jacobian and the generalized mass matrix of the robot, respectively, $\mathbf{q}$ is the joint position vector, and $\mathbf{e}_j$ is a unitary vector defined as follows

$$\mathbf{e}_j = \begin{cases} \begin{bmatrix} 1 & 0 & 0 & 0 & 0 & 0 \end{bmatrix}^T & \text{for the } x \text{ direction} \\ \begin{bmatrix} 0 & 1 & 0 & 0 & 0 & 0 \end{bmatrix}^T & \text{for the } y \text{ direction} \\ \begin{bmatrix} 0 & 0 & 1 & 0 & 0 & 0 \end{bmatrix}^T & \text{for the } z \text{ direction} \end{cases}$$

Similarly, the equivalent stiffness K_{r_j} in the j-th Cartesian direction ($j = x$, y, z), depending on the robot configuration $\mathbf{q}$, is given by [40]

$$K_{r_j} = \frac{1}{\mathbf{e}_j^T \mathbf{C}_{ee} \mathbf{e}_j}$$

where the end-effector compliance $\mathbf{C}_{ee}$ is composed by two different contributions, one related to lumped joint compliance and the other one due to distributed arm stiffness, i.e.,

$$\mathbf{C}_{ee} = \mathbf{C}_J + \mathbf{C}_L$$

The joint compliance matrix $\mathbf{C}_J$ is defined as follows [40]

$$\mathbf{C}_J = \mathbf{J}_A(\mathbf{q}) \mathbf{K}_J^{-1} \mathbf{J}^T(\mathbf{q})$$

where $\mathbf{J}_A(\mathbf{q})$ is the analytic robot Jacobian and $\mathbf{K}_J = \text{diag}\{k_1, \ldots, k_N\}$ is the diagonal matrix of the joint stiffnesses k_j, $j = 1, \ldots, N$, N being the number of links.

On the other side, the i-th link compliance matrix is given by [40]

$$\mathbf{C}_{L_i} = \mathbf{A}_{L_i}(\mathbf{q})^T \mathbf{K}_{L_i}^{-1} \mathbf{A}_{L_i}(\mathbf{q})$$

where $\mathbf{A}_{L_i}(\mathbf{q})$ is a transformation matrix from the absolute reference frame to the i-th link reference frame defined as

$$\mathbf{A}_{L_i}(\mathbf{q}) = \begin{bmatrix} {}^o\mathbf{R}_{L_i}(\mathbf{q}) & \mathbf{0} \\ \mathbf{0} & {}^o\mathbf{R}_{L_i}(\mathbf{q}) \end{bmatrix} \begin{bmatrix} \mathbf{I}_3 & \mathbf{0} \\ [\mathbf{r}_i]_\times & \mathbf{I}_3 \end{bmatrix}$$

with ${}^o\mathbf{R}_{L_i}(\mathbf{q})$ the rotation matrix from the absolute reference frame to the reference frame of the i-th link, $\mathbf{r}_i \in \mathbb{R}^3$ the distance vector from the external end of the i-th link to the end-effector position, and $[\mathbf{r}_i]_\times \in \mathbb{R}^{3\times 3}$ the matrix performing the cross product

$$[\mathbf{r}_i]_\times \mathbf{x} = \mathbf{r}_i \wedge \mathbf{x} \qquad \forall \mathbf{x} \in \mathbb{R}^3$$

The stiffness of the i-link, modelled as an Euler-Bernoulli beam [40], with respect

to its local reference frame is given by

$$\mathbf{K}_{L_i} = \begin{bmatrix} 12p & 0 & 0 & 0 & -6L_ip & 0 \\ 0 & 12q & 0 & 6L_iq & 0 & 0 \\ 0 & 0 & L_i^2r & 0 & 0 & 0 \\ 0 & 6L_iq & 0 & 4L_i^2q & 0 & 0 \\ -6L_ip & 0 & 0 & 0 & 4L_i^2p & 0 \\ 0 & 0 & 0 & 0 & 0 & L_i^2u \end{bmatrix}$$

$$p = EI_{x,i} \qquad q = EI_{y,i} \qquad r = EA_i \qquad u = GI_{z,i}$$

where E and G are the Young modulus and the shear modulus characterising the link material, respectively, $I_{x,i}$, $I_{y,i}$ and $I_{z,i}$, are the moments of inertia of the cross-sectional area of the beam A_i, and L_i is the length of the link.
Finally, the total link compliance matrix $\mathbf{C}_L$ is defined as follows

$$\mathbf{C}_L = \sum_{i=1}^{N} \mathbf{C}_{L_i}$$

where N is the number of links.

Note that, the stability analysis here presented does not change if a reference signal is added to the system in Figure 3.
In particular, an additional virtual force, like the one generated by a virtual constraint [1], can be considered without affecting the stability of the closed-loop system. Furthermore, a position (orientation) reference $\bar{\mathbf{p}}_P$ ($\bar{\mathbf{r}}_P$) can be added as well, recasting it, thanks to a suitable impedance filter, into a force (torque) reference.

5. Experimental results

All the experiments, related to human arm parameter identification and hands-on control, have been performed with a Comau Smart Six industrial robot equipped with an ATI Gamma SI-130-10 force/torque sensor and an aluminium handling tool (Figure 6). The robot is controlled by a C4GOpen industrial controller, that allows an external real-time Linux PC, connected through a

2 ms real-time Ethernet link, to close some of the motion control loops.
In this specific application, the external PC is used to close an admittance loop around the industrial controller joint position loops, and to log force/torque and joint measurements.

Using an industrial robot has pros and cons. The main disadvantage is that Smart Six, as any industrial manipulator, is massive and bulky and thus both parameter identification and hands-on control experiments, requiring the human operator to be in close collaboration with the robot, can be very dangerous. On the other side, considering that hands-on control has important applications in industrial robot programming, using Smart Six allows to test the approach in a realistic scenario. Furthermore, Smart Six mechanical chain is characterised by lumped flexibilities, at all the joints, and distributed flexibilities, especially at the fourth link. Some hands-on control experiments revealed joint oscillations close to the stability limit when the operator moves the robot forward and backward in the plane including joints 2, 3 and 5. This makes Smart Six a perfect test bench to show the effectiveness of the approach here proposed.

Figure 6: The handling tool used to perform identification and hands-on experiments.

5.1. Human arm identification

5.1.1. Experimental protocol

First of all, human arm impedance of three different subjects [27, 37], males with an average age of 31 years, an average height of 182 cm, and all right-handed (more details are reported in Table 1), has been experimentally identified. Following the experiments performed in [37], the set-up (Figure 7(a)) has been organized as follows:

- a chair has been located in front of the robot, kept always at the same position, where a person can sit down and grasp the end-effector handling tool keeping a comfortable position, i.e., without co-contracting muscles;
- five different postures have been used, corresponding to different end-effector positions (see Table 2 and Figures 7(b)- 7(f)), but all characterised by the same height with respect to ground.

Subject	Gender	Age [years]	Height [m]	Right/left handed
1	male	41	1.75	right-handed
2	male	25	1.85	right-handed
3	male	28	1.87	right-handed

Table 1: Characteristics of the subjects used for human arm impedance identification.

Position	${}^{o}x$[m]	${}^{o}y$[m]	${}^{o}z$[m]
P_1	0.80	0.10	1.06
P_2	0.95	0.00	1.06
P_3	0.95	0.10	1.06
P_4	0.95	0.20	1.06
P_5	1.10	0.10	1.06

Table 2: Positions for human arm impedance identification, coordinates with respect to absolute robot frame.

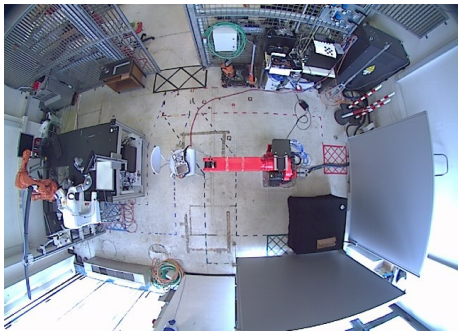

(a) experimental setup

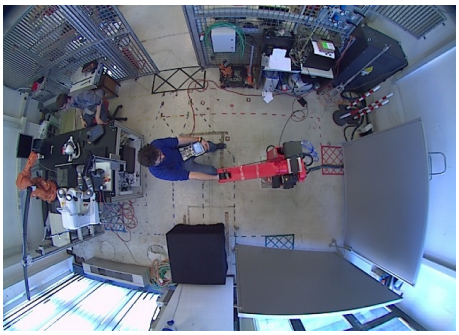

(b) position P_1

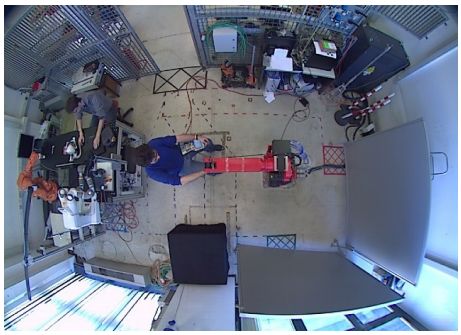

(c) position P_2

(d) position P_3

(e) position P_4

(f) position P_5

Figure 7: The experimental setup and the five positions used for human arm impedance identification.

Before each test, the human has been instructed to sit down on the chair and hand the tool without co-contracting muscles, keeping, as much as possible, a planar human arm configuration, i.e., with shoulder center, elbow and wrist in the same plane parallel to the ground plane. Moreover, subjects have been asked to avoid looking at their hands during the identification experiment in order to limit the effect of possible undesired muscle activations [31].

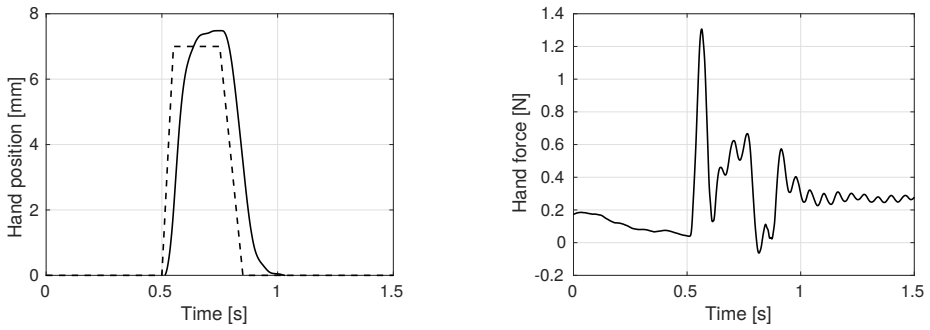

(a) position profile

(b) human arm reaction

Figure 8: An example of stimulus for human arm impedance identification (position reference as a dashed line, actual position as a solid line), and the corresponding human arm force response recorder by the sensor.

In order to identify the human arm impedance, the robot performs a very small motion in the x and y directions recording the reaction of the human arm in terms of force in both directions [27]. Differently from [27], however, a trapezoidal space profile, instead of a square wave, has been adopted, mainly for safety reasons. The trapezoidal wave is characterised by a constant velocity of 0.14 m/s for 0.05 s, zero velocity for 0.2 s, and a negative velocity of 0.07 m/s for 0.1 s at the end (Figure 8). Using a trapezoidal instead of a square wave space profile allows to limit the maximum required end-effector velocity, in this way a reasonable safety threshold can be set on the robot Cartesian velocity, triggering an emergency stop in case this value is exceeded.

A complete test is constituted by 5 cycles, each one characterised by a trapezoid in the x and another one in the y direction, and between two consecutive cycles a

break of ten seconds is performed. The same test is executed twice, the first time instructing the subject to avoid muscle co-contraction ($\sigma = 0$), the second time asking him/her to co-contract his/her muscles as much as he/she can ($\sigma = 1$). Figure 9 shows an example of 5 cycles recorded from a subject avoiding muscle co-contraction.

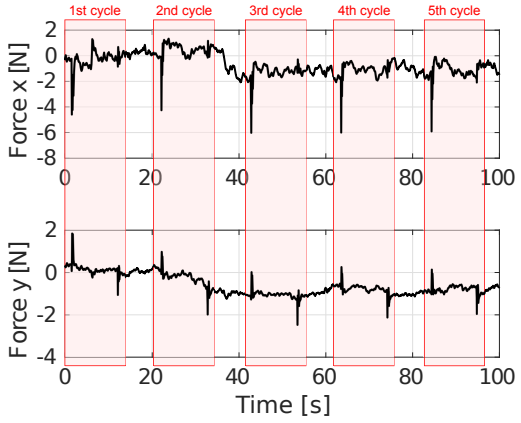

Figure 9: Human arm reaction as recorded by the force sensor in a complete experiment constituted by 5 cycles.

5.1.2. Identification results

A complete dataset is composed of five pulses in the x direction and five in the y direction for each co-contraction index, and by the corresponding responses of the human arm in terms of hand force in both directions (Figure 11).

As can be seen from Figure 8(b) the human arm response to a stimulus lasts approximately half a second, in spite of that only the first 100 ms, characterized by the visco-elastic response of the human arm (Figure 10), are usually exploited to identify stiffness [27]. In the experiments here considered, however, this procedure yields sometimes erroneous results, i.e., a negative stiffness, as it has already been reported in [8]. For this reason, a window of 200 ms, including secondary reflexes but excluding voluntary motion, has been used (Figure 10). Moreover, hand forces are normalised subtracting the initial values, i.e., the average forces computed in a time window of 30 ms before the perturbation

onset.

Given end-effector position, velocity, acceleration, and hand force, human arm mass, stiffness and damping matrices can be estimated using a linear regression technique. In fact, the model in equation (1) can be expressed in identification form as follows

$$\underbrace{\mathbf{F}_h\left(\mathbf{q}_h, t\right)}_{\mathbf{F}} = \underbrace{\begin{bmatrix}\mathbf{M}_h(\mathbf{q}_h,t) & \mathbf{D}_h(\mathbf{q}_h,t) & \mathbf{K}_h(\mathbf{q}_h,t)\end{bmatrix}}_{\mathbf{\Pi}} \underbrace{\begin{bmatrix}\ddot{\mathbf{q}}_h \\ \dot{\mathbf{q}}_h \\ \mathbf{q}_h\end{bmatrix}}_{\mathbf{Y}}$$

Then, given m measurements, the previous relation can be rewritten as

$$\mathbf{F}_m = \mathbf{\Pi}\mathbf{Y}_m$$

where $\mathbf{F}_m$ is the vector of m force measurements, and $\mathbf{Y}_m$ the vector of m position, velocity and acceleration measurements.

Matrix $\mathbf{\Pi}$ can be thus computed as

$$\mathbf{\Pi} = \mathbf{F}_m \mathbf{Y}_m^{\dagger}$$

where $\mathbf{Y}_m^{\dagger}$ is the right pseudoinverse of $\mathbf{Y}_m$.

Tables 3 and 5 report the average (among the five pulses) stiffness and damping matrix elements for the three subjects and the five positions. Figure 14, instead, shows a validation of the human arm impedance model referred to subject 2 and posture 4. As it can be clearly seen, the force predicted by the human arm model is in good accordance with the five experimentally recorded force reactions, especially considering the complexity of the human arm neuromuscular system and the simplicity of the model. Moreover, as it can be seen in the figure, a delay of 100 ms, representing the reaction time, has been introduced.

Using data in Table 3, the symmetric part of the stiffness matrix can be determined and computing eigenvalues and eigenvectors the stiffness ellipsoids associated to each position can be derived. Figure 12 shows these ellipsoids for the first subject.

Note that, as reported in literature [41, 26], the ellipsoid principal axes are

Subject 1

Posture	K_{xx} [N/m]	K_{yy} [N/m]	K_{xy} [N/m]	K_{yx} [N/m]
1	618.08	15.90	− 87.66	−114.98
2	416.47	16.28	−145.96	−178.69
3	297.98	18.64	−142.18	−129.71
4	306.82	33.54	− 58.16	− 89.84
5	252.89	50.47	−133.79	−161.42

Subject 2

Posture	K_{xx} [N/m]	K_{yy} [N/m]	K_{xy} [N/m]	K_{yx} [N/m]
1	1304.92	47.76	− 91.46	− 95.12
2	366.07	9.89	− 90.19	−106.31
3	358.91	5.32	− 80.48	−122.62
4	402.06	32.06	− 54.49	− 69.67
5	208.04	29.14	−140.29	−147.97

Subject 3

Posture	K_{xx} [N/m]	K_{yy} [N/m]	K_{xy} [N/m]	K_{yx} [N/m]
1	545.05	6.00	−136.67	−133.99
2	180.36	5.37	− 91.38	− 83.88
3	224.14	13.20	−102.50	−103.14
4	213.16	1.29	− 55.10	− 80.62
5	169.53	26.65	−129.72	− 93.11

Table 3: Results of human arm stiffness identification on the three subjects.

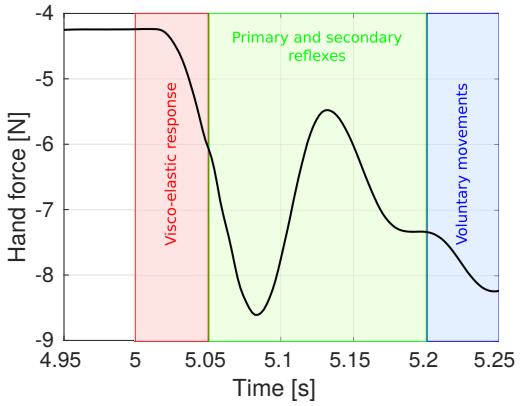

Figure 10: Time intervals used in the human arm response analysis.

	F_x		F_y	
	P_1, P_3, P_5	P_2, P_3, P_4	P_1, P_3, P_5	P_2, P_3, P_4
b_1	9900.0	2047.7	954.6	876.8
b_2	-20851.0	-477.7	-1766.7	-124.1
b_3	11168.0	321.0	823.7	10.5
a	266.0		50.0	

Table 4: Results of human arm model averaged on the three subjects.

Subject 1

Posture	D_{xx} [Ns/m]	D_{yy} [Ns/m]	D_{xy} [Ns/m]	D_{yx} [Ns/m]
1	35.51	11.47	−10.07	−12.88
2	26.05	16.90	−12.70	−13.66
3	34.39	13.40	−10.85	−10.02
4	34.18	10.51	− 6.70	− 7.15
5	28.54	13.74	− 9.68	− 8.81

Subject 2

Posture	D_{xx} [Ns/m]	D_{yy} [Ns/m]	D_{xy} [Ns/m]	D_{yx} [Ns/m]
1	40.53	11.31	− 8.25	− 5.52
2	30.59	21.30	−12.97	−12.52
3	38.48	15.20	−12.54	−11.17
4	45.85	11.27	− 8.77	− 7.58
5	27.05	18.63	−15.05	−11.21

Subject 3

Posture	D_{xx} [Ns/m]	D_{yy} [Ns/m]	D_{xy} [Ns/m]	D_{yx} [Ns/m]
1	29.21	12.15	−13.61	−12.03
2	16.71	20.70	− 9.15	− 7.96
3	24.03	13.88	−11.19	−11.02
4	25.20	12.24	− 8.34	− 8.86
5	21.30	17.34	−11.94	−10.14

Table 5: Results of human arm damping identification on the three subjects.

directed towards the shoulder position. Moreover, it can be also noticed that the ellipsoid corresponding to posture P_1 has a principal axis with a length that is definitely greater with respect to the other ones, this is due to the fact that this human arm configuration is very close to a singularity, where the estimated stiffness is due not only to muscles, but also to bones.

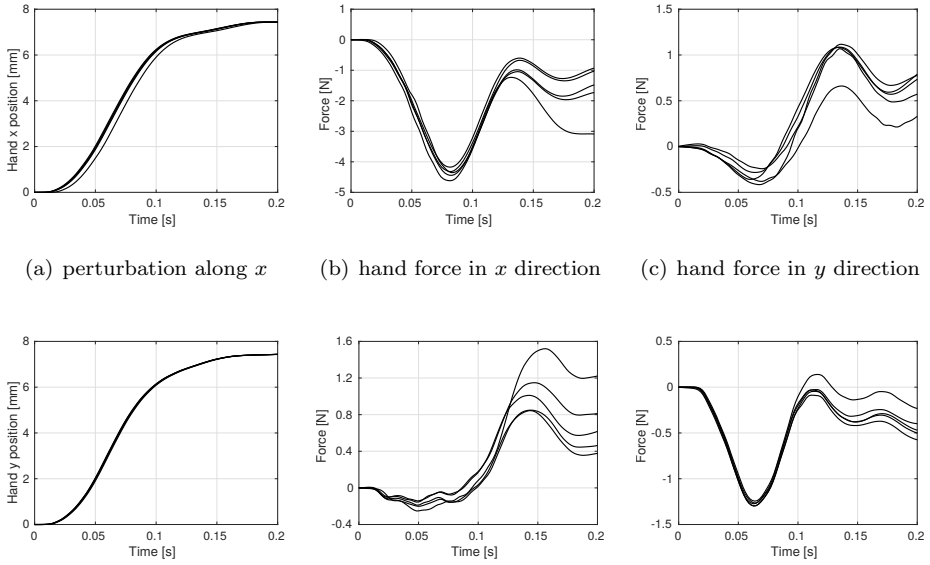

(a) perturbation along x (b) hand force in x direction (c) hand force in y direction

(d) perturbation along y (e) hand force in x direction (f) hand force in y direction

Figure 11: An example of complete experiment composed of 5 cycles.

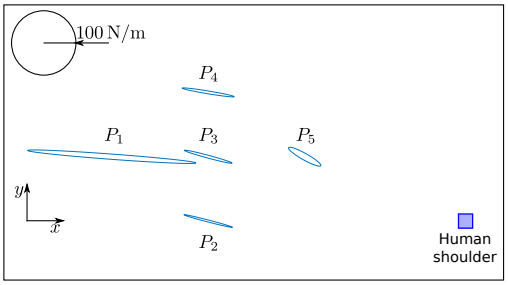

Figure 12: Stiffness ellipsoids for subject 1.

Exploiting again data in Table 3 and the model introduced in Section 3, the

human arm impedance relation along a linear path in the x or y directions can be derived[4].

Figures 15 and 16 show the stiffness-position relation for a linear path along positions P_1, P_3, P_5 and P_2, P_3, P_4, respectively (Figure 13), while Table 4 reports the corresponding values of the coefficients a, b_1, b_2, b_3, that define the arm impedance relation (2) of an average model among the three subjects.

Using a combination of the two models, the behaviour of the stiffness along a circular path (Figure 13) has been also determined (Figure 17).

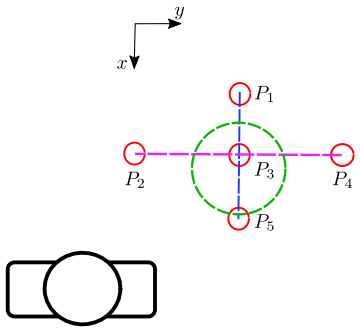

Figure 13: Linear and circular paths used for hands-on control experiments.

5.2. Admittance filter tuning

Given the human arm stiffness model described in Section 3, the manipulator stiffness matrices as reported in [40], and applying the procedure introduced in Section 4, the minimum damping that stabilises the system for three different values of the virtual tool mass – 2 Kg, 25 Kg, 50 Kg –, and for the five human arm postures considered in the identification process can be determined.

Gains are reported in Table 6.

Note that, the damping associated to posture P_1 is definitely larger with respect to that of the other postures. This is due to the fact, already observed

[4]The same approach can be used to derive the damping-position and mass-position relations, that are not reported here as only the stiffness is required to compute the admittance filter gains.

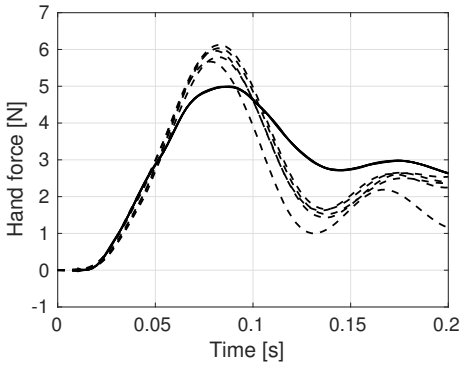

Figure 14: Validation of human arm impedance for subject 2 in posture 4 (force predicted by the model as a solid line, experimental data as dashed lines.

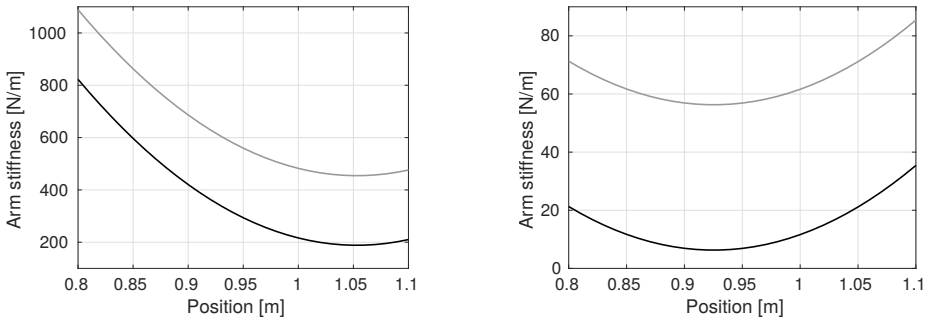

(a) K_{xx} (b) K_{yy}

Figure 15: Human arm stiffness model for a linear path along positions P_1, P_3, P_5 ($\sigma = 0$, black solid line; $\sigma = 1$, gray solid line).

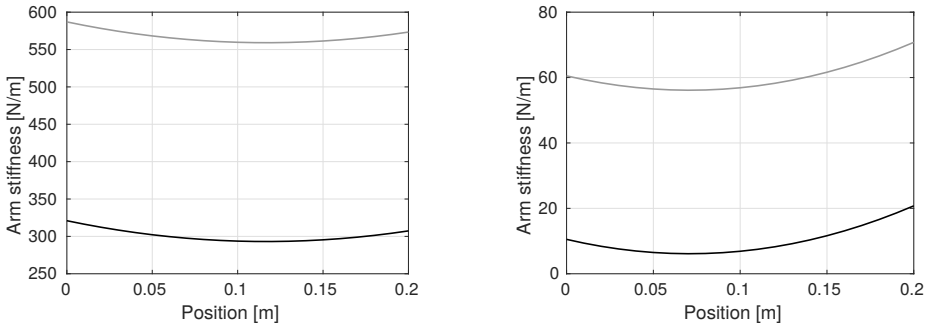

(a) K_{xx} (b) K_{yy}

Figure 16: Human arm stiffness model for a linear path along positions P_2, P_3, P_4 ($\sigma = 0$, black solid line; $\sigma = 1$, gray solid line).

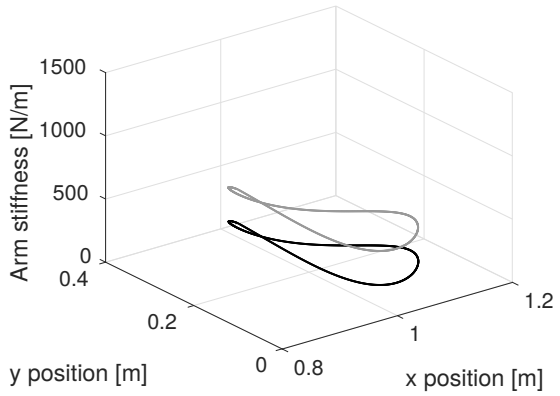

Figure 17: Human arm stiffness model for a circular path ($\sigma = 0$, black solid line; $\sigma = 1$, gray solid line).

$1-3-5$	M [Kg]	D_x [Ns/m]	D_y [Ns/m]
P_1	2	174	35
	25	266	60
	50	705	85
P_3	2	111	23
	25	177	42
	50	352	56
P_5	2	87	40
	25	139	74
	50	290	98

$2-3-4$	M [Kg]	D_x [Ns/m]	D_y [Ns/m]
P_2	2	58	30
	25	88	54
	50	193	71
P_3	2	49	28
	25	72	41
	50	160	67
P_4	2	54	42
	25	51	77
	50	179	102

Table 6: Admittance filter gains for the different postures.

in Section 5.1.2, that stiffness in P_1 is larger with respect to stiffness of all other postures.

5.3. Hands-on control experiments

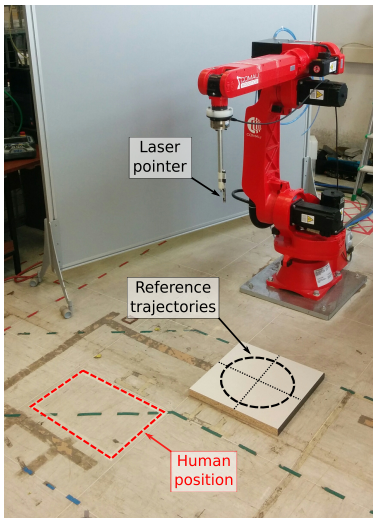

Figure 18: The experimental setup used for the hands-on control experiments.

Hands-on control experiments have been performed asking human operators to stand still in front of the robot, in a place marked by a rectangle on the floor (Figure 18), grasping the handling tool. To allow the execution of comparable trajectories by different operators, a laser pointer has been attached to the handling tool and two linear and one circular paths have been drawn on the floor (Figure 18). The operator, thanks to the pointer projecting a laser spot on the floor, follows these guidelines performing similar trajectories along different experiments.

Multiple tests have been performed, considering linear and circular paths and different masses of the virtual tool. As the aim of these tests is to assess the validity, including the robustness, of the proposed admittance controller tuning methodology, the paths performed by the operators are similar but not identical to the ones considered for the identification step. For example, a path along P_2, P_3, P_4 is a line parallel to the y-axis, and thus to the segment used

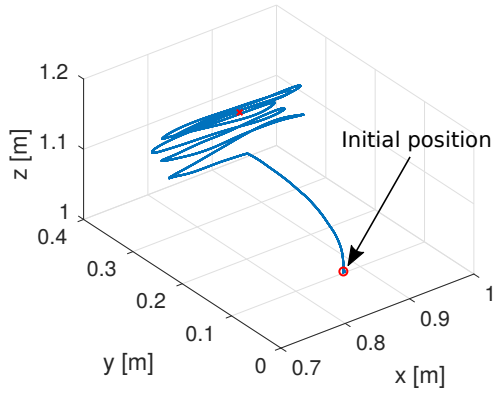

Figure 19: Hand path in an hands-on control experiment along P_1, P_3, P_5.

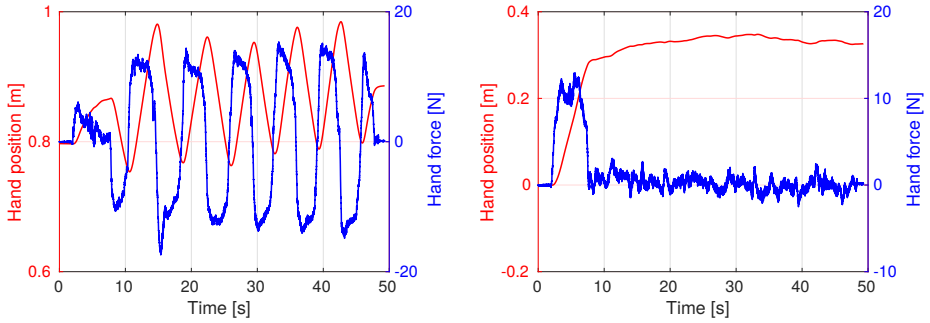

(a) x direction

(b) y direction

Figure 20: Hand positions and forces in an hands-on control experiment along P_1, P_3, P_5.

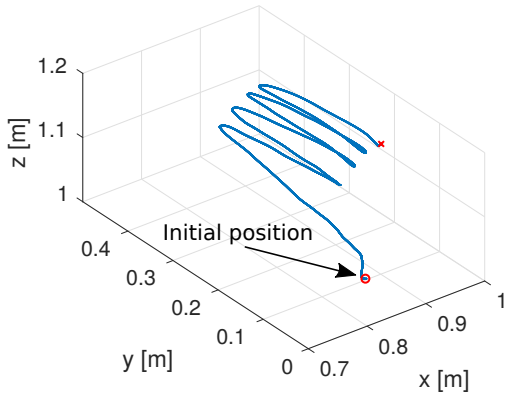

Figure 21: Hand path in an hands-on control experiment along P_2, P_3, P_4.

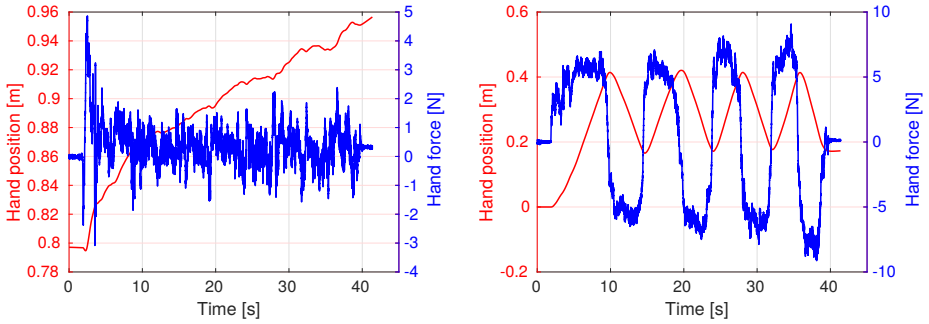

(a) x direction (b) y direction

Figure 22: Hand positions and forces in an hands-on control experiment along P_2, P_3, P_4.

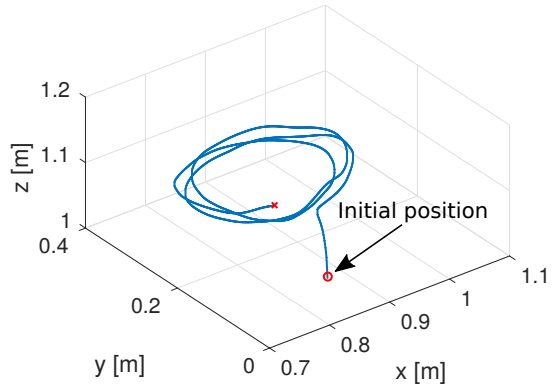

Figure 23: Hand path in an hands-on control experiment along a circular path.

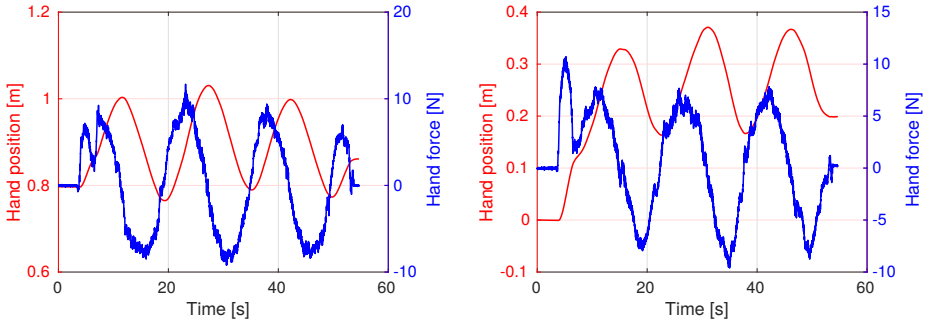

(a) x direction (b) y direction

Figure 24: Hand positions and forces in an hands-on control experiment along a circular path.

for identification purposes, having a similar but not equal length. In conclusion, if the identification pattern guarantees that sufficient data are available to characterise the arm impedance model for both the x and y directions over the region of the robot workspace required to perform the task, the operator is then free to move along all this region with a guarantee on the stability of the human-robot interaction.

In the following, the results of two repeated linear paths and one repeated circular path, with a virtual mass of 25 Kg for the linear path along P_2, P_3, P_4 and of 50 Kg for the linear path along P_1, P_3, P_5 and the circular path, are reported. In particular, Figures 20 and 22, and Figures 19 and 21 show the forces, the end-effector displacements and 3D paths for the linear movements along the x and y directions, i.e., points P_1, P_3, P_5 and P_2, P_3, P_4, respectively. Figures 23 and 24, instead, show the same variables for the circular trajectory.

In both experiments the human operator has not perceived any anomalous vibration, nor it is evident from measured forces or positions.

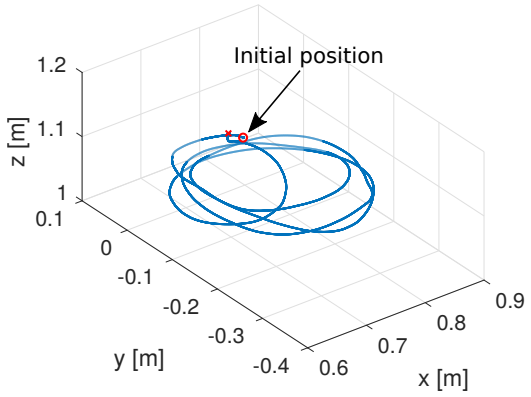

Figure 25: Hand path in an hands-on control experiment along a circular path with low virtual mass.

The results of another test, characterised by a virtual tool mass of 2 Kg, are shown in Figures 25 and 26. Such a low mass represents a very critical situation, especially during the inversion of the direction of motion, i.e., when the end-effector velocity is close to zero and the stabilising effect of the damping

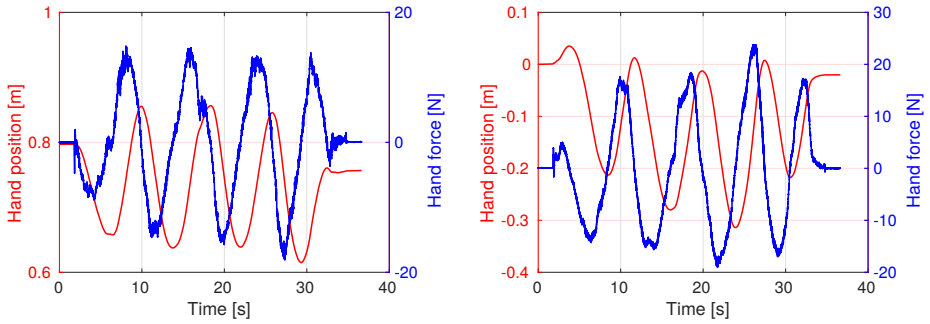

(a) x direction (b) y direction

Figure 26: Hand positions and forces in an hands-on control experiment along a circular path with low virtual mass.

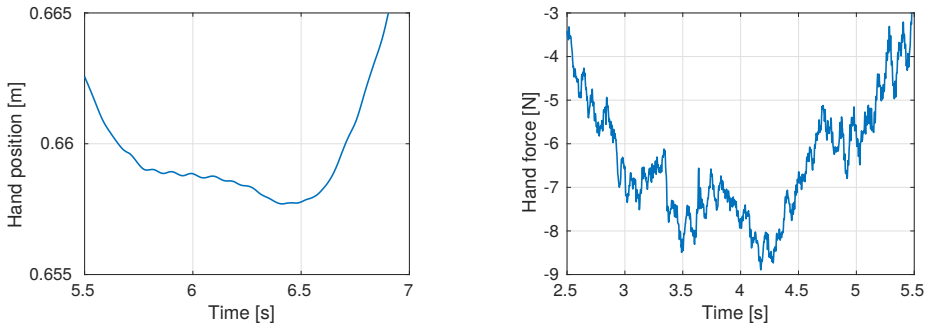

(a) hand x-position (b) hand force

Figure 27: Hands-on control experiment along a circular path with low virtual mass, x-position and force during the inversion of the direction of motion.

component vanishes. Nevertheless, as it can be seen in Figure 27, even in this situation vibrations are very small and almost indiscernible by the human operator.

345 *5.4. Exploiting the human arm impedance model*

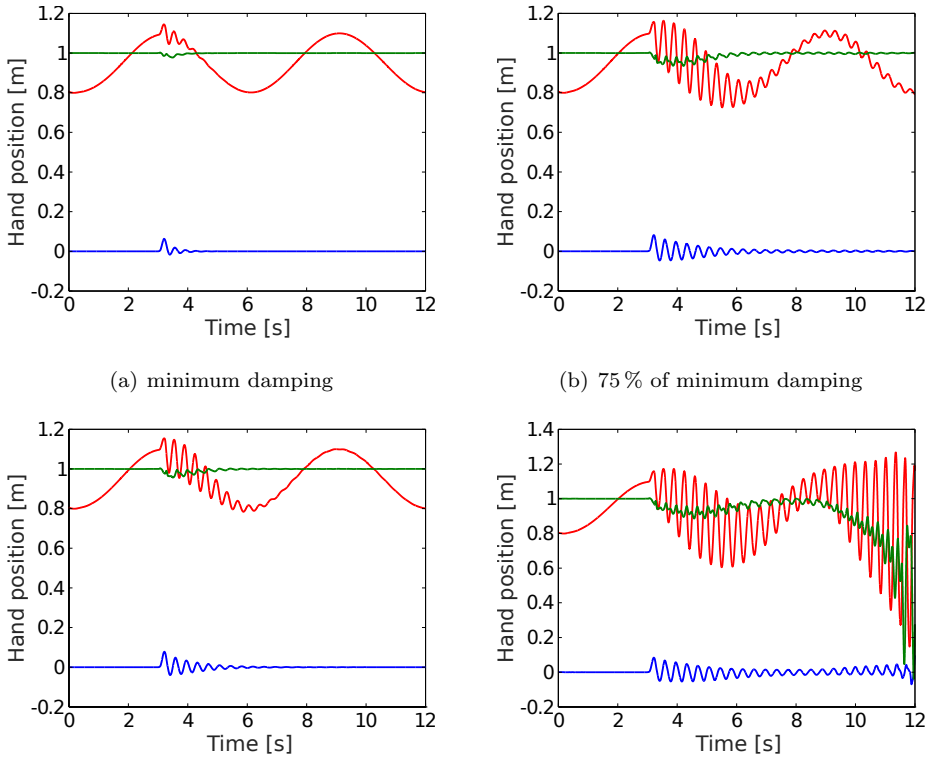

(a) minimum damping

(b) 75 % of minimum damping

(c) 70 % of minimum damping

(d) 67.5 % of minimum damping

Figure 28: Simulated 3D hand position for different admittance filter dampings.

The nonlinear model reported in Section 3 allows to draw some conclusions related to a possible drawback of the presented approach, i.e., an excessive human effort caused by the increased value of the admittance filter damping used to enforce stability. To show that this does not represent an issue, a sinusoidal
350 motion of the human hand has been simulated considering values of the admittance filter damping above and below the minimum determined by the stability

analysis[5]. Moreover, a force disturbance of 30 N, almost ten times higher then the one recorded during the identification experiments, has been injected after 3 seconds to verify the stability.

Figure 28 shows the 3D hand position for the minimum damping (Figure 28(a)), and for a damping of 75 % (Figure 28(c)), 70 % (Figure 28(b)) and 67.5 % (Figure 28(d)) the minimum one. As it can be clearly seen, the response of the system to the force disturbance moves from well-damped oscillations, when the minimum damping ensuring asymptotic stability is applied, to diverging oscillations, i.e., instability.

Furthermore, these four simulations allow to compare the human effort related to different values of the admittance filter damping. In Table 7 the maximum force and the work required to execute the task are reported.

Though the difference, in terms of work, between the minimum damping that ensures stability of the closed-loop system and 67.5 % of this value is significant (there is an increase of approximately 50 %), it must be noticed that 6.45 J is the energy required to lift a mass of 1 Kg for 62 cm, being thus a definitely little effort.

D	F_{max}	W
[Ns/m]	[N]	[J]
41.00	6.07	6.45
30.75	4.55	4.84
28.70	4.25	4.52
27.68	4.10	4.36

Table 7: Forces and human effort for different damping values.

Finally, using the human arm impedance model and the elastic model of the robot introduced in Section 4, one can compute the minimum damping

[5] As this comparison involves the use of damping coefficients that do not ensure stability, for safety reasons it cannot be performed on the experimental system.

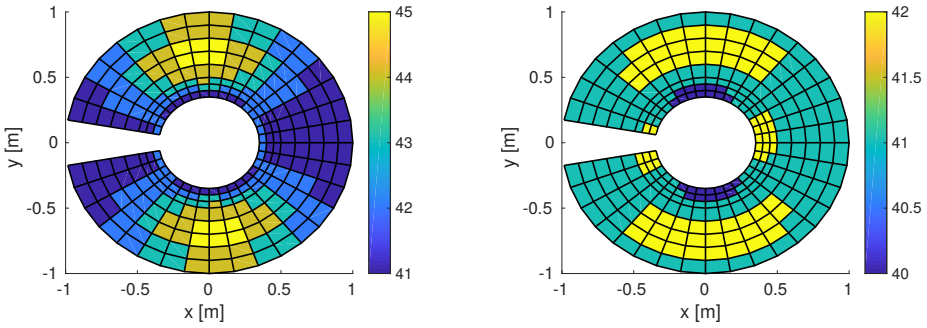

(a) 0.45 m

(b) 0.55 m

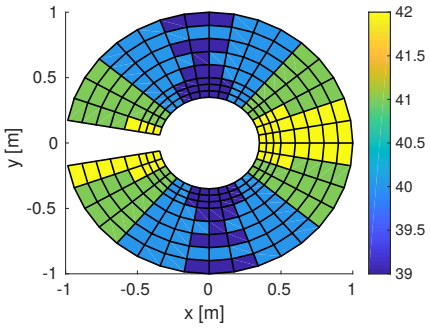

(c) 0.70 m

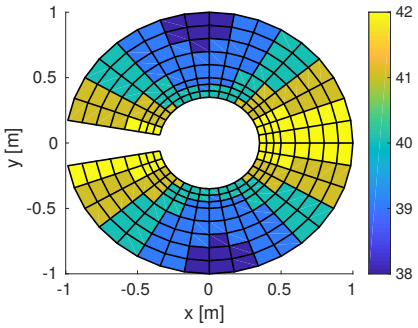

(d) 1.00 m

Figure 29: Minimum damping of the admittance filter in the robot workspace, for different end-effector heights.

ensuring stability of the closed-loop system for different robot configurations in the robot workspace. This allows to draw the charts in Figure 29 that, for each motion along the x-axis at a given and constant height, and starting from a particular robot configuration, give the minimum damping of the admittance filter. In other words, these charts give an intuitive representation of the risk of instability associated to each zone of the robot workspace.

6. Conclusions

This paper presents a novel methodology, based on absolute stability theory, to assess the stability of the human-robot interaction during hands-on control tasks. Thanks to a nonlinear but simplified model of the human arm impedance, whose parameters can be easily experimentally identified using least-squares techniques, the admittance filter can be designed in such a way that the stability is always ensured.

The experimental results confirm that the selected impedance model, though simplified, is suitable to characterise the human arm reactions during human-robot interaction, and to assess the system stability. Moreover, hands-on control tests reveal that the proposed designed methodology is able to guarantee stability, and thus absence of vibrations during the execution of the task, without causing an excessive human effort. This allows to improve the safety and comfortability, reducing the psychological stress, of the human operator, increasing the accuracy of the executed task, as well.

Finally, the proposed methodology opens the way to the design of an adaptive admittance filter that, thanks to a continued online human arm impedance identification, ensures robust asymptotic stability and accuracy of the hands-on control task.

Acknowledgement

The authors would like to thank former student G. Frasca for her valuable work on this project.

References

[1] L. Bascetta, G. Ferretti, G. Magnani, P. Rocco, Walk-through programming for robotic manipulators based on admittance control, Robotica 31 (2013) 1143–1153.

[2] Y. Aydin, O. Tokatli, V. Patoglu, C. Basdogan, Stable physical human-robot interaction using fractional order admittance control, IEEE Transactions on Haptics 11 (3) (2018) 464–475.

[3] S.-Y. Li, I. Paranawithana, L. Yang, T. S. K. Lim, S. Foong, F. C. Ng, U.-X. Tan, Stable and compliant motion of physical humanrobot interaction coupled with a moving environment using variable admittance and adaptive control, IEEE Robotics and Automation Letters 3 (3) (2018) 2493–2500.

[4] I. Ranatunga, F. L. Lewis, D. O. Popa, S. M. Tousif, Adaptive admittance control for human-robot interaction using model reference design and adaptive inverse filtering, IEEE Transactions on Control Systems Technology 25 (1) (2017) 278–285.

[5] B. Yao, Z. Zhou, L. Wang, W. Xu, Q. Liu, A. Liu, Sensorless and adaptive admittance control of industrial robot in physical human-robot interaction, Robotics and Computer Integrated Manufacturing 51 (2018) 158–168.

[6] E. Guiffo Kaigom, J. Roßmann, Physics-based simulation for manual robot guidance – an erobotics approach, Robotics and Computer Integrated Manufacturing 43 (2017) 155–163.

[7] M. Ragaglia, A. M. Zanchettin, L. Bascetta, P. Rocco, Accurate sensorless lead-through programming for lightweight robots in structured environments, Robotics and Computer Integrated Manufacturing 39 (2016) 9–21.

[8] M. S. Erden, A. Billard, End-point impedance measurements at human hand during interactive manual welding with robot, in: IEEE International Conference on Robotics and Automation, 2014, pp. 126–133.

[9] A. Campeau-Lecours, P.-L. Belzile, T. Laliberté, S. Foucault, B. Mayer-St-Onge, D. Gao, C. Gosselin, An articulated assistive robot for intuitive hands-on-payload manipulation, Robotics and Computer Integrated Manufacturing 48 (2017) 182–187.

[10] P.D. Labrecque, C. Gosselin, Variable admittance for pHRI: From intuitive unilateral interaction to optimal bilateral force amplification, Robotics and Computer Integrated Manufacturing 52 (2018) 1–8.

[11] J. G. Petersen, S. A. Bowyer, F. R. y. Baena, Mass and friction optimization for natural motion in hands-on robotic surgery, IEEE Transactions on Robotics 32 (1) (2016) 201–213.

[12] F. Ficuciello, L. Villani, B. Siciliano, Variable impedance control of redundant manipulators for intuitive human-robot physical interaction, IEEE Transactions on Robotics 31 (4) (2015) 850–863.

[13] V. Okunev, T. Nierhoff, S. Hirche, Human-preference-based control design: Adaptive robot admittance control for physical human-robot interaction, in: IEEE International Symposium on Robot and Human Interactive Communication, 2012, pp. 443–448.

[14] C. Wang, Y. Li, S. S. Ge, K. P. Tee, T. H. Lee, Continuous critic learning for robot control in physical human-robot interaction, in: International Conference on Control, Automation and Systems, 2013, pp. 833–838.

[15] T. Tsumugiwa, R. Yokogawa, K. Hara, Variable impedance control based on estimation of human arm stiffness for human-robot cooperative calligraphic task, in: IEEE International Conference on Robotics and Automation, Vol. 1, 2002, pp. 644–650.

[16] H. Modares, I. Ranatunga, F. L. Lewis, D. O. Popa, Optimized assistive human-robot interaction using reinforcement learning, IEEE Transactions on Cybernetics 46 (3) (2016) 655–667.

[17] B. Alqaudi, H. Modares, I. Ranatunga, S. M. Tousif, F. L. Lewis, D. O. Popa, Model reference adaptive impedance control for physical human-robot interaction, Control Theory and Technology 14 (1) (2016) 68–82.

[18] I. Ranatunga, S. Cremer, D. O. Popa, F. L. Lewis, Intent aware adaptive admittance control for physical human-robot interaction, in: IEEE International Conference on Robotics and Automation, 2015, pp. 5635–5640.

[19] T. Tsuji, Y. Tanaka, Tracking control properties of human-robotic systems based on impedance control, IEEE Transactions on Systems, Man, and Cybernetics - Part A: Systems and Humans 35 (4) (2005) 523–535.

[20] K. Ohta, M. M. Svinin, Z. Luo, S. Hosoe, R. Laboissière, Optimal trajectory formation of constrained human arm reaching movements, Biological Cybernetics 91 (1) (2004) 23–36.

[21] M. Svinin, K. Ohta, Z. W. Luo, S. Hosoe, Towards understanding of human movements constrained by the external environment, in: IEEE/RSJ International Conference on Intelligent Robots and Systems), Vol. 1, 2003, pp. 155–161.

[22] A. Q. Keemink, H. van der Kooij, A. H. Stienen, Admittance control for physical humanrobot interaction, International Journal of Robotics Research.

[23] V. Duchaine, C. M. Gosselin, Investigation of human-robot interaction stability using lyapunov theory, in: IEEE International Conference on Robotics and Automation, 2008, pp. 2189–2194.

[24] H. K. Khalil, Nonlinear Systems, Pearson Education, 2000.

[25] H. Patel, G. O'Neill, P. Artemiadis, On the effect of muscular cocontraction on the 3-D human arm impedance, IEEE Transactions on Biomedical Engineering 61 (10) (2014) 2602–2608.

[26] F. A. Mussa-Ivaldi, N. Hogan, E. Bizzi, Neural, mechanical, and geometric factors subserving arm posture in humans, The Journal of Neuroscience 5 (10) (1985) 2732–2743.

[27] S. Abiko, A. Konno, M. Uchiyama, An asymmetric stiffness model of a human hand, in: IEEE/RSJ International Conference on Intelligent Robots and Systems, 2010, pp. 5034–5041.

[28] K. Tahara, H. Kino, Iterative learning control for a redundant musculoskeletal arm: acquisition of adequate internal force, in: IEEE/RSJ International Conference on Intelligent Robots and Systems, 2010, pp. 234–240.

[29] J. M. Dolan, M. B. Friedman, M. L. Nagurka, Dynamic and loaded impedance components in the maintenance of human arm posture, IEEE Transactions on Systems, Man and Cybernetics 23 (3) (1993) 698–709.

[30] S. Wang, G. Zuo, J. Xu, H. Zheng, Human hand impedance characteristics during reaching movements, in: International Conference on Biomedical Engineering and Informatics, Vol. 3, 2011, pp. 1282–1286.

[31] T. Tsuji, P. G. Morasso, K. Goto, K. Ito, Human hand impedance characteristics during maintained posture, Biological Cybernetics 72 (6) (1995) 475–485.

[32] N. Hogan, The mechanics of multi-joint posture and movement control, Biological Cybernetics 52 (5) (1985) 315–331.

[33] H. Gomi, R. Osu, Task-dependent viscoelasticity of human multijoint arm and its spatial characteristics for interaction with environments, The Journal of Neuroscience 18 (21) (1998) 8965–8978.

[34] M. M. Rahman, R. Ikeura, K. Mizutani, Investigating the impedance characteristic of human arm for development of robots to co-operate with human operators, in: IEEE International Conference on Systems, Man, and Cybernetics, Vol. 2, 1999, pp. 676–681.

[35] A. Schouten, E. de Vlugt, J. van Hilten, F. van der Helm, Quantifying proprioceptive reflexes during position control of the human arm, IEEE Transactions on Biomedical Engineering 55 (1) (2008) 311–321.

[36] X. Lamy, F. Colledani, F. Geffard, Y. Measson, G. Morel, Achieving efficient and stable comanipulation through adaptation to changes in human arm impedance, in: IEEE International Conference on Robotics and Automation, 2009, pp. 265–271.

[37] H. S. Woo, D. Y. Lee, Exploitation of the impedance and characteristics of the human arm in the design of haptic interfaces, IEEE Transactions on Industrial Electronics 58 (8) (2011) 3221–3233.

[38] G. Frasca, Analisi di stabilitá dell'interazione uomo-robot nelle operazioni collaborative di manual guidance, Master's thesis, Politecnico di Milano (2015).

[39] O. Khatib, Advanced robotics manipulation, lecture Notes of the course (2005).

[40] R. Rossi, L. Bascetta, P. Rocco, Implicit force control for an industrial robot with flexible joints and flexible links, in: IEEE/RSJ International Conference on Intelligent Robots and Systems, 2014, pp. 4742–4749.

[41] N. Hogan, Impedance control: An approach to manipulation, in: American Control Conference, 1984, pp. 304–313.